June 27, 2011

TECP Calibration Report

Doug Cobos (Decagon Devices), Steve Wood (University of Washington), Aaron Zent (NASA Ames Research Center)

I. Introduction

This document describes the calibration of the flight TECP units. The calibration methods and results are discussed, as well as other relevant information that could affect the accuracy of the various measurements while being performed on Mars. The TECP measurement functions will be described individually below, and the current calibrations at time of launch for the flight unit #004 will be highlighted in red to aid readability.

Three flight TECP units were assembled at JPL; #004, #010, and #012. Originally, units #004 and #012 were chosen as flight and flight spare respectively. A calibration campaign was conducted at JPL in May 2006, where #004 and #012 were fully calibrated according to the TECP calibration plan. It was later noticed that the process of cleaning and conformal coating the PCBs of #004 resulted in significant change in the low range electrical conductivity (EC) measurements at very high impedances. As a result, the decision was made to replace #004 with the flight spare, #012. In January 2007, a second calibration campaign was conducted at JPL which consisted of a full re-calibration of the EC function of #012, a checkout of the other functions of #012 to ensure that they had not changed as a result of the conformal coating, and a nearly full calibration of the remaining flight unit #010. After #012 was swapped on to the robotic arm, it suffered a power-up while its connector was mis-mated during ATLO. Concern that the #012 electronics may have been damaged forced unit #004 to be re-designated as the flight unit. A quick re-calibration of the EC function was performed at Lockheed before #004 was placed back on the robotic arm. Therefore #004 was the unit flown to Mars, #012 suffered damage to a digital component which should not invalidate any of the calibrations performed on it. Unit #010 is partially-calibrated, and is being used in characterization studies.

II. Board (PCB) Temperature Sensor Calibration

A. May 2006 Calibration

Overview

The PCB (board) temperature sensors on the TECP flight unit and flight spare (#004 and #012) were calibrated to NIST-traceable temperature standards. The board temperature sensor calibration was a two part process. Opening the flight units and attaching temperature sensors directly to the boards was not an acceptable option, so an EM unit was used to characterize the temperature difference between the board temperature and the temperature at the outside of the TECP enclosure on the analog board cover directly above the board temperature sensor. NIST traceable temperature references were then attached to the flight TECP units above the board temperature sensors and the housing temperature was measured while the TECP was brought to temperatures over its full expected temperature range. The correction determined on the EM unit was applied to derive the board temperature, and the calibration function was determined.

Experimental

Part 1

EM R-2 unit #001 was used to characterize the temperature difference between the analog board and the external surface of the TECP housing directly above board temperature sensor. Chromel constantan thermocouples were attached with kapton tape to the analog PCB, adjacent to the board temperature sensor, and to the analog board cover directly above the other thermocouple. Unit #001 was then placed in an aluminum thermal enclosure, which was in turn placed in a Delta Design environmental test chamber. The chamber was used to bring the thermal enclosure and TECP to equilibrium at six temperatures: 158 K, 173 K, 213 K, 233 K, 263 K, and 296 K (-113°C, -100°C -60°C -40°C, -10°C, 23°C). Raw voltage output from the two thermocouples was recorded with a National Instruments SCXI-1000 thermocouple system. TECP board temperature sensor data were also collected at 1Hz through the TECP-IF interface. The TECP unit remained powered-up between measurements. The raw thermocouple data were converted to temperature using the standard published Seebeck coefficient data for chromel constantan thermocouple wire.

The time-series thermocouple data were studied after a step change in temperature to determine how long the TECP should be allowed to soak to achieve complete thermal equilibrium. These data showed that board temperature and the temperature gradient between the PCB and the analog board cover both stabilize within 25 minutes of commanded changes to the chamber temperature. For all of the tests in Part 2, the TECP units were allowed to soak for at least 30 minutes at each temperature before data were analyzed.

Part 2

Diode type, NIST traceable temperature sensors (Lake Shore Cryotronics model DI-470) were attached with kapton tape to the TECP analog board covers directly above the board temperature sensors. The TECP units were placed in the aluminum thermal enclosure in the Delta Design chamber. The chamber was used to bring the thermal enclosure and TECP to equilibrium at nine temperatures: 160 K, 180 K, 200 K, 220 K, 240 K, 260 K, 280 K, and 303 K (-113 °C, -93 °C, -73 °C, -53 °C, -33 °C, -13 °C, 7 °C, and 30 °C). A Lake Shore model 331 temperature controller was used to collect raw voltage output from the diode sensors at 1Hz.

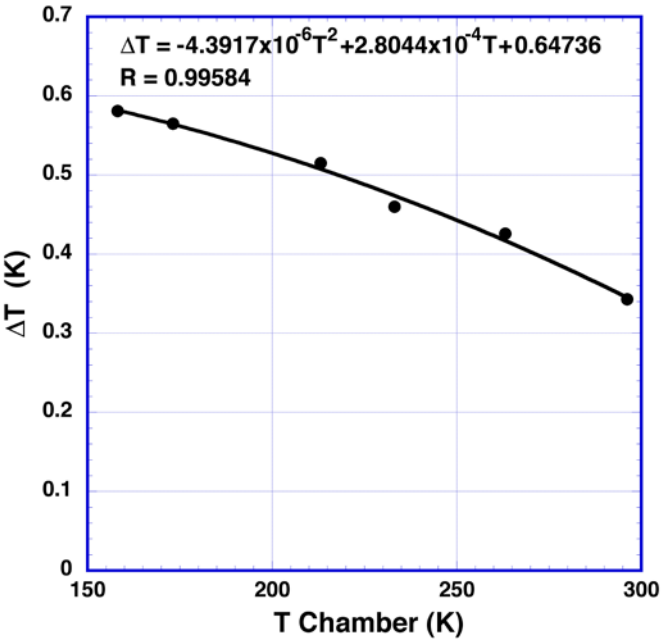

Figure 1. Temperature difference between TECP PCB and analog board cover as a function of setpoint temperature.

TECP PCB temperature sensor data were also collected at 1Hz through the TECP-IF interface. The raw diode output was converted to temperature using the calibration sheets accompanying each sensor. During post-processing, the difference between board temperature and analog cover temperature determined in Part 1 were applied to the temperatures measured by the diode sensors.

Results

Part 1

The temperature gradient between the PCB and the analog board cover varied as a function of temperature (data file: *TECP EM Tboard - Tcover.xls*). The temperature gradient decreased as chamber temperature increased (Figure 1). This is presumably caused by the lower frequency of blasts of chilled nitrogen by the Delta Design chamber at higher temperatures. Even though the TECP was in a thermal enclosure, there were large grooves cut into the walls of the chamber to accommodate lead wires, which allowed convective heat exchange during the blasts of nitrogen. At higher temperatures, the less frequent blasts allowed the TECP to become more isothermal, while at low temperatures, the TECP housing was cooled by forced convection generating a steeper temperature gradient between the PCB and the analog board cover. The polynomial model of this relationship shown in Figure 1 was applied to the calibration data in Part 2.

Part 2

Figures 2 and 3 show the calibration functions for TECP units #004 and 012 respectively (data file: *TECP PCB temperature calibration.xls*). There is a linear relationship between the board temperature sensor output and the board temperature for both units, but substantially different offsets between the two sensors.

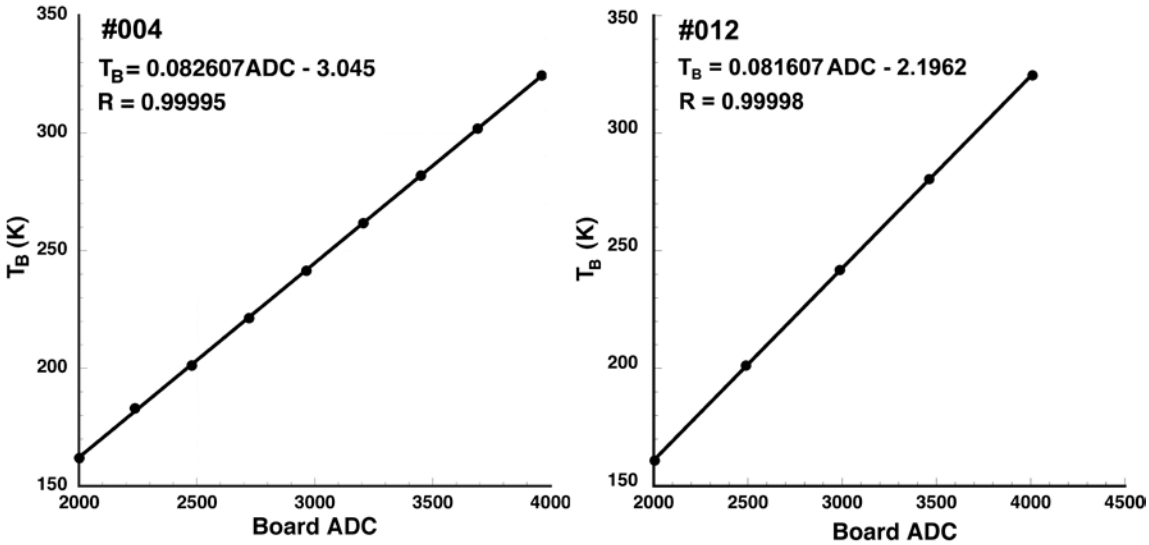

Figures 2 and 3. Board temperature sensor calibration for TECP unit #004 (left) and TECP unit #012 (right).

B. January 2007 Calibration

Overview

During the January, 2007 calibration campaign the PCB temperature sensor of unit #012 and #010 were calibrated in the manner described above. For unit #012, this constituted a calibration check, while this was the only board temperature sensor calibration performed on #010.

Experimental

The same apparatus and experimental protocols were used in the Jan 07 trial as were described for the May 06 trial above

Results

The calibration function generated for unit #012 with the Jan 07 data is very similar to that generated with the May 06 data. The agreement between the two calibrations was checked by applying the both the May 06 and Jan 07 calibration functions to the data collected during the Jan 07 calibration check and comparing. The standard error between the two resulting data sets is less than 0.005 C. This indicated a negligible change in the PCB temperature sensor calibration on unit #012 resulting from cleaning and conformal coating.

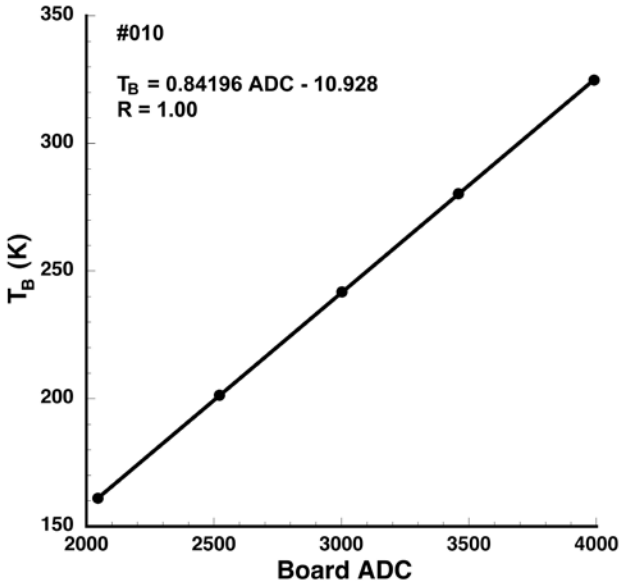

Figure 4. TECP unit #010 board temperature sensor calibration.

Figure 4 shows the calibration function for TECP unit #010 (data file: *TECP 010 and 012 PCB temp cal.xls*). There is a linear relationship between the board temperature sensor output and the board temperature.

III. Thermocouple Calibration

Overview

The objective of this experiment was to determine the Seebeck coefficient vs. temperature for the thermocouple alloys used in the TECP needles. This allows allow accurate determination of the temperature difference between the TECP needles and the reference temperature at the TECP PCB. It should be noted that this is the only calibration activity that was performed at the Decagon Devices facility. It should also be noted that the cleaning and conformal coating of the TECP PCBs should not affect this calibration since it is strictly a property of the thermocouple wire composition.

Experimental

Two cylindrical pieces of copper 1.3 cm long x 4.6 cm diameter were used as test blocks with the purpose of holding a thermocouple junction and temperature sensor in a stable,

isothermal environment (see Figure 5). The two blocks were bolted 6.5 cm apart on a piece of acrylic, which was set on top of a block of open cell foam in a Delta Design environmental test chamber. The two blocks each had a 3.2 mm diameter hole bored to their center from the rounded surface, which housed pre-calibrated temperature sensors and thermocouple junctions (refer to the document titled "CR7 thermocouple calibration.doc," 6/21/05 for documentation on the NIST traceable temperature sensors referenced here).

The thermocouple for which the Seebeck coefficient function was derived was constructed from the spool of material used by East30 Sensors to fabricate the TECP needle thermocouples in all three flight units. The thermocouple was fabricated by soldering the ends of a 7.5 cm piece of constantan thermocouple wire to the ends of two 75 cm pieces of chromel thermocouple wire using Kester Sn63Pb37 rosin core solder and Indium Flux #1. The thermocouple junctions and NIST-traceable temperature sensors were co-located and potted in the borehole in the copper blocks with Arctic Silver high thermal conductivity grease.

The chromel thermocouple leads were routed through a mousehole in the door of the Delta Design chamber and were soldered with Kester Sn63Pb37 rosin core solder to 12 AWG stranded copper wires that terminated in tinned leads. The chromel/copper solder junctions created here were clamped into screw terminals that were mounted onto a 5 cm long x 4.6 cm diameter copper block with Arctic Alumina high thermal conductivity 5 minute epoxy. To ensure that these two junctions remained at the same temperature, the copper block and screw terminals were insulated in a four-piece closed cell foam chamber custom cut for this purpose. The foam chamber was further protected from heat exchange with a cardboard convection shield.

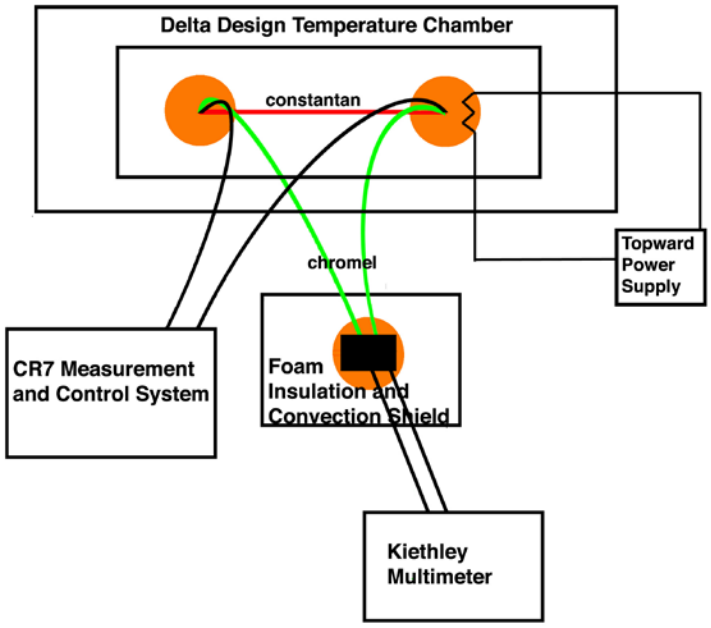

Figure 5. Schematic of thermocouple calibration test setup.

In one of the blocks, a 0.4 cm hole was bored completely through the block to facilitate an electrical heating element to allow the block temperature to be controlled independently of the second block, and thus achieve a temperature difference between the two thermocouple junctions. The heater was a 180 ohm resistor with leads soldered to two 122 cm pieces of 14 AWG stranded copper wire. The resistor was potted in the borehole with Arctic Silver high thermal conductivity

grease, and the leads were electrically isolated from the copper block with heat shrink tubing, and were routed through a mousehole in the door of the Delta Design chamber.

A Campbell Scientific CR7 measurement and control system (SN 2147) was used to collect data from the temperature sensors in the isothermal blocks. Refer to the document tiled "CR7 thermocouple calibration.doc" for documentation on the calibration procedure and NIST traceability of the temperature sensors and CR7 data acquisition system. The temperatures were read from a laptop in serial communication with the CR7, and recorded in an Excel spreadsheet *Flight thermocouple calibrations.xls*. A Keithley model 2001 (SN 555318) multimeter was used to read the μV response of the thermocouple, and the results were recorded in the Excel spreadsheet. The multimeter was calibrated at Keithley Inc. to NIST traceable standards on 6/14/05. A Topward Electric Instruments model TPS-4000D digital DC power supply was used to provide power to the heating element in the heated copper block.

The Delta Design temperature chamber was used to control the temperature of the atmosphere around the copper test blocks containing the thermocouple junctions and temperature sensors. Seebeck coefficients were determined for the thermocouple at approximately 30 K increments from 150 to 330 K. The blocks were allowed to equilibrate at each ambient temperature setting for at least 30 minutes. At each ambient temperature, the Topward power supply was used to apply between 0 and 32 V to the resistor in the heated copper block producing a temperature difference (ΔT) between the two blocks. At least four ΔTs were produced at each chamber temperature. At each ΔT setting, the voltage control on the Topward power supply was manually adjusted to stabilize the temperature difference at the desired level. At least 60 seconds were allowed to pass between the final voltage adjustment and the recording of data to ensure that the system was in thermal equilibrium.

Results

Figure 6 shows the Seebeck coefficient vs. temperature data collected here. The data closely follow a third order polynomial function shown on the graph (data file: *TECP thermocouple calibration.xls*). The Seebeck coefficient function shown here should be used to calculate the temperature difference between the needles and the board temperature sensor on the flight units.

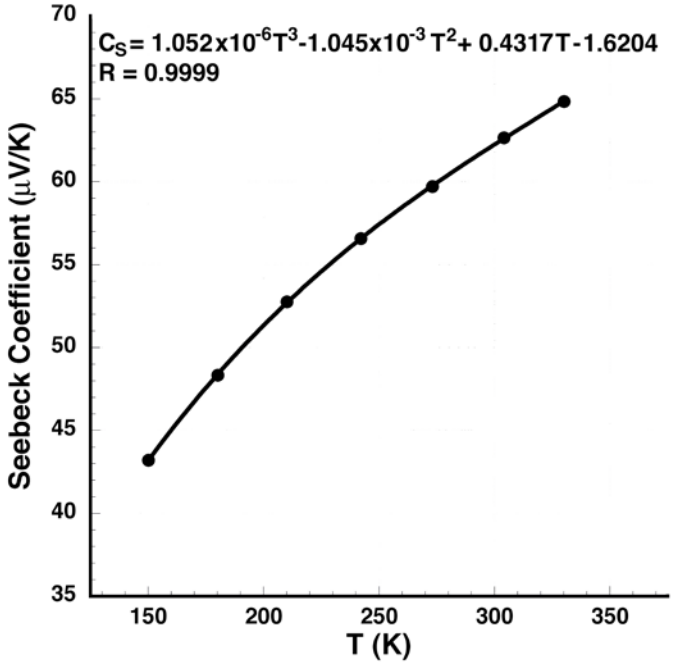

Figure 6. Seebeck coefficient function for TECP flight units.

IV. Dielectric

Function Calibration

A. May 2006 Calibration

Overview

The objective of this procedure was to construct TECP dielectric output vs. known dielectric permittivity functions for TECP units #004 and #012.

Experimental

TECP dielectric measurements were taken in a series of four fluids with relative dielectric permittivities from 1 to 20 (Table 1). Each of the fluids was housed in a 30.4 cm diameter by 17.5 cm depth glass bowl, filled to within 1 cm of the top. Earlier finite element analysis and experimental testing showed that >95% of the electromagnetic field generated by the TECP dielectric measurement was contained within this volume of any of the four fluids. All measurements were performed in a drybox under dry N_2 purge, with the TECP lowered into the fluids with a translation stage. The TECP units were inserted into the fluid until the needles and PEEK shoulders were submerged. For the air, isopropyl, and 1-decanol samples, the fluids were allowed to equilibrate to the temperature of the drybox for at least 1 hour prior to data collection. The tert-butanol sample was held at a steady, above-ambient temperature with an electrical heating pad due to its high melting temperature (28 °C). In each fluid, data were collected from the TECP unit for 25 minutes to assure thermal equilibrium between the needles and the fluid. Thermal drift was not identified in any of the samples after one minute of equilibration time, so the TECP output values presented below are the averages of approximately the final 24 minutes of data collection.

Table 1. Nominal dielectric permittivity of TECP calibration fluids

Material	Nominal dielectric
Air	1
1-decanol	7.5
Tert butanol	10.9
Isopropyl	18.3

Prior to making TECP measurements in the fluids, six sub samples of each of the three measured alcohols were collected. The fluids were transferred to 100 ml septa-equipped, airtight glass containers in the drybox under N_2 purge. The relative dielectric permittivity of the samples was independently determined at the TECP calibration temperatures at the NIST Dielectric and Magnetic Material lab. The NIST characterizations were performed at the same measurement frequency as the TECP dielectric measurement (6.25 MHz). Two separate parallel plate devices were used in the NIST characterization.

Results

The TECP output and true relative dielectric permittivities determined by the NIST lab are shown in Table 2 (data file: *NIST dielectric calibrations.pdf*). Note that the dielectric permittivities reported here are the averages of the values measured by the two NIST parallel plate instruments. In no case was the difference between the two values greater than 0.3%.

Table 2. Results of TECP dielectric calibration and NIST alcohol characterization.

Material	T (°C)	Dielectric	Output #004 (ADC)	Output #012 (ADC)
Air	23	1	642	552
1-decanol	24	8.07	1410	1328
Tert butanol #004	32	11.22	2300	
Tert butanol #012	30.5	11.49		2290
Isopropyl	23	19.76	4016	4016

Using the data in Table 2, calibration functions were determined for each of the two TECP units (Figures 7 and 8). The shapes of the best fit calibration functions are very similar for the two units, but are both nonlinear (data files: *TECP #4 dielectric calibration.xls* and *TECP #12 dielectric calibration.xls*).

B. January 2007 Calibration

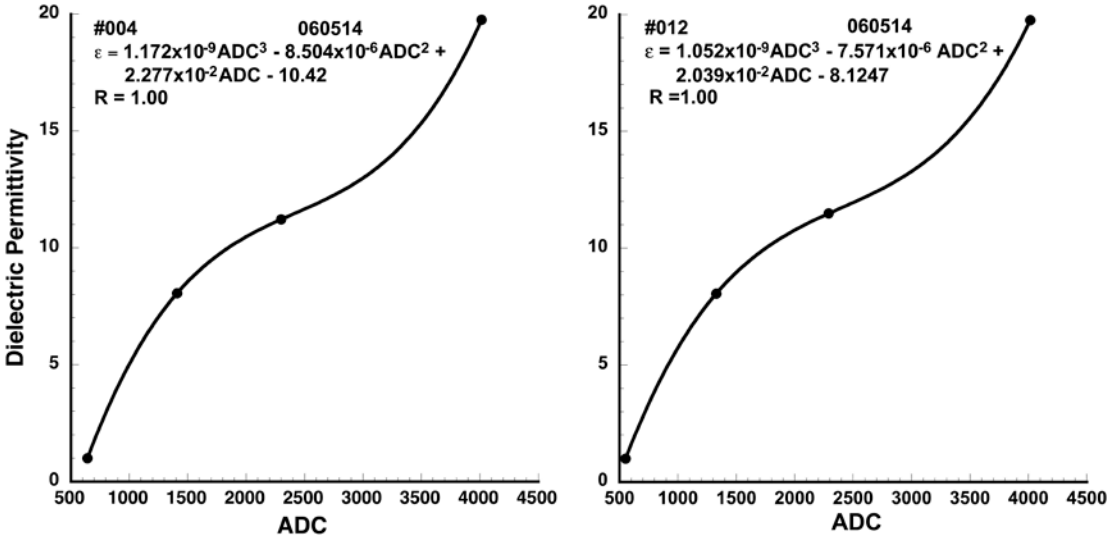

Figures 7 and 8. Dielectric permittivity calibration for unit #004 and unit #012. March, 2006 calibration.

Overview

During the January 2007 re-calibration of #012, a brief investigation was conducted to quantify any possible changes in the dielectric function. Additionally a two-point calibration was performed on #010. Unfortunately, the data collection was interrupted, so a complete dielectric calibration has not been performed on #010 to date.

Experimental

TECP unit #012 originally underwent a full calibration of its dielectric function in May 2006. The methods and results are above. In the January, 2007 re-calibration of the EC function, the dielectric function of unit #012 was re-checked in two of the four fluids included in the original calibration: air and 1-decanol. Additionally, unit #010 was calibrated in the same two fluids. The same apparatus and experimental protocols were used in the Jan 07 trial as were described for the May 06 trial. The one exception to direct comparability is that instead of virgin 1-decanol, the same 1-decanol from the first trial was re-used during the second trial. 1-decanol is hygroscopic, and will scavenge water vapor from the atmosphere if exposed to moist air. All measurements during both

trials were done under dry N_2 purge, preventing moisture sorption during those times. However, it is possible that a small amount of water vapor could have been taken up while the 1-decanol was being removed from the glovebox after the first trial, and during the storage period between trials. The effect of water vapor sorption would be an increase in the dielectric constant of the fluid.

Results

The dielectric measurement of unit #012 in air showed an increase of about 16 ADC (Table 3). This is almost certainly a result of the conformal coating increasing the dielectric constant of the space near the trace that carries the dielectric excitation signal from the oscillator to the pad where the electrical connection is made to the needle. It is well known that fringing will create a small electromagnetic field near the surface of the PCB where these traces lie, and that any non-air material on the surface of the board will increase the detected dielectric constant of the circuit. In the 1-decanol, the dielectric measurement increased by about 23 ADC. Although this would seem to be a significantly larger increase than in air, it may not be. Very slight differences in insertion depth into the 1-decanol bath would result in a 7 ADC change in output above what was seen in air. Also, any sorption of water vapor could also increase the dielectric constant of the 1-decanol itself. The most likely mechanism for dielectric function output increase is the added capacitance from the conformal coating on the PCB. This should manifest itself as an offset increase to the calibration function. The new unit #012 calibration equation, adjusted from the original in the manner indicated above is included in Figure 10. Table 4 shows the two point calibration performed on unit #010 in January 07. Additional data points will be required to fully calibrate the dielectric function of unit #010.

Table 3. TECP #012 Dielectric ADC Output: Air and Decanol: May ’06 – Jan ‘07

Medium	T fluid (°C)	ADC May 06	ADC Jan 07	Δ	NIST e
air	22.9	552.0	568.0	16.0	1.00
1-decanol	24.3	1327.7	1350.3	22.6	8.06

Table 4. TECP #010: Dielectric ADC Output; January ‘07

T fluid (°C)	ADC: Jan ‘07	Δ	NIST ε
22.6	502.4	1.0	1.00
24.1	1249.0	7.5	8.06

After conformal coating, TECP unit #004 underwent checkout testing, which included exercising the dielectric function in air. The dielectric function output increased by 7 ADC over the pre conformal coating value. A new calibration model has been calculated including this offset (Figure 10).

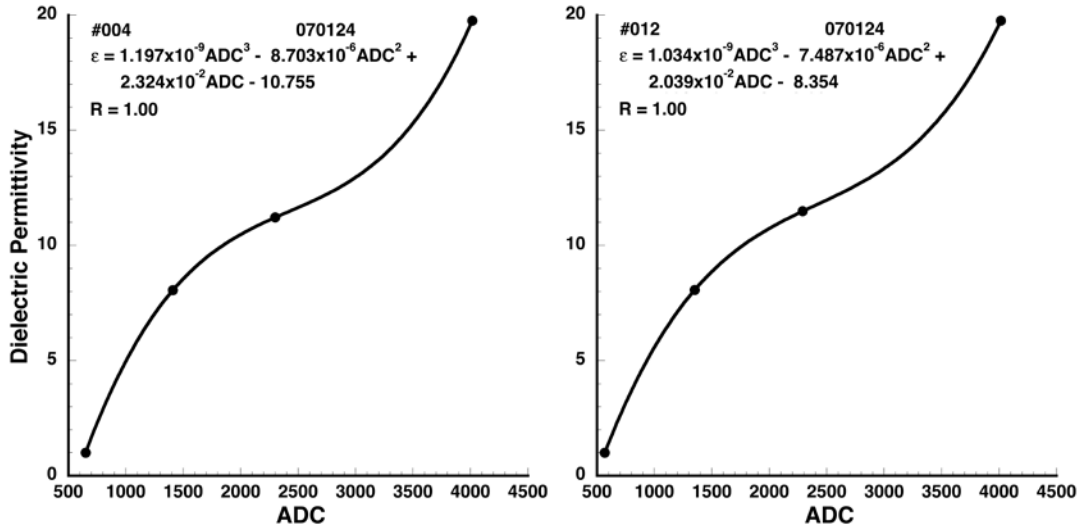

Figures 9 and 10. Dielectric permittivity calibration for unit #004 and unit #012. January, 2006 calibration.

C. In-Flight Temperature Calibration

Because the TECP operated over a much greater temperature range than it was possible to calibrate over, and because of the lack of suitable permittivity standards for Mars-like temperatures, a simple temperature correction was made by running the dielectric measurement function in air, both during calibration, and on the Martian surface. The relative permittivity of air is unity, independent of temperature.

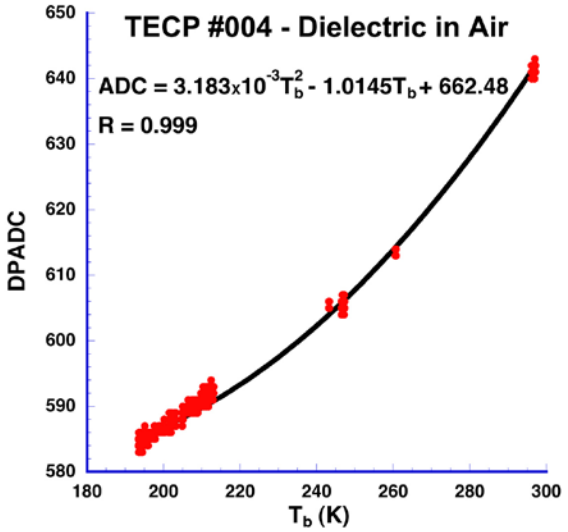

Figure 11. TECP calibration and flight data, acquired in air.

Figure 11 shows the ADC output in air, plotted against the electronics board temperature. The data, including the calibration data, are best fit by a 2nd-order polynomial.

The quantity to add to the ADC output value is expressed as the following function of the board temperature

$$\Delta ADC = -3.183x10^{-3} T_b^2 + 1.0145 T_b - 20.48 \qquad (1)$$

The resulting number should be added to the raw ADC output prior to applying the calibration function given in Figure 9.

V. Thermal Properties Calibration

A. May 2006 Calibration

Overview

The TECP thermal properties measurement functions were calibrated at the system level. Measurements in materials of known thermal properties were used to construct a calibration function for the thermal conductivity measurement and volumetric heat capacity measurement for each flight TECP unit in a manner described in Cobos et al., (2006) and summarized here.

Experimental

Materials

TECP thermal properties time series data sets were collected in five materials with known thermal properties (Table 5). The Macor ceramic, HDPE, and glycerol were obtained from commercial vendors. The EPS was obtained from a larger block of certified material used as a thermal conductivity calibration standard at Decagon. The water was stabilized with agar powder at a mixing ratio of 5g agar/l water to prevent free convection from the heating of the needles.

In the case of the stabilized water and glycerol, thermal property values were taken from published reference literature. The thermal properties of the Macor and HDPE samples were determined with a commercial thermal properties meter (model KD2 Pro, Decagon Devices), which was calibrated immediately prior to testing. The EPS material is a commercially available, NIST-traceable thermal conductivity standard material obtained from LaserComp, Inc. The volumetric specific heat of the foam standard was calculated calorimetrically from published values of the specific heat and density of polystyrene and the measured density of the EPS.

Table 5. Thermal properties standard materials used in the TECP calibration.

Material	κ (W m^{-1} K^{-1})	Source	C(MJ m^{-3} K^{-1})
Macor (glass ceramic, 25 °C)	1.402	Decagon	2.01
Water (stabilized, 25 °C)	.608	CRC	4.17
High density polyethylene (HDPE, 23 °C)	0.513	Decagon	1.69
Glycerol (20 °C)	0.285	Ganic & Hicks	2.96
Expanded polystyrene (EPS, 20 °C)	0.033	Laser Comp	0.063

Data collection

All measurements were taken in a drybox using a vertical stage to insert the TECP needles into the standard materials. There was no N_2 purge for any of the materials except glycerol, which is hygroscopic. The stabilized water and glycerol were housed in 600 ml beakers, into which the TECP was lowered until the metal sensing needles were fully immersed in the fluid, but the PEEK shoulders were not. The TECP sensing needles were inserted into the EPS (Styrofoam) block using the vertical stage, and were

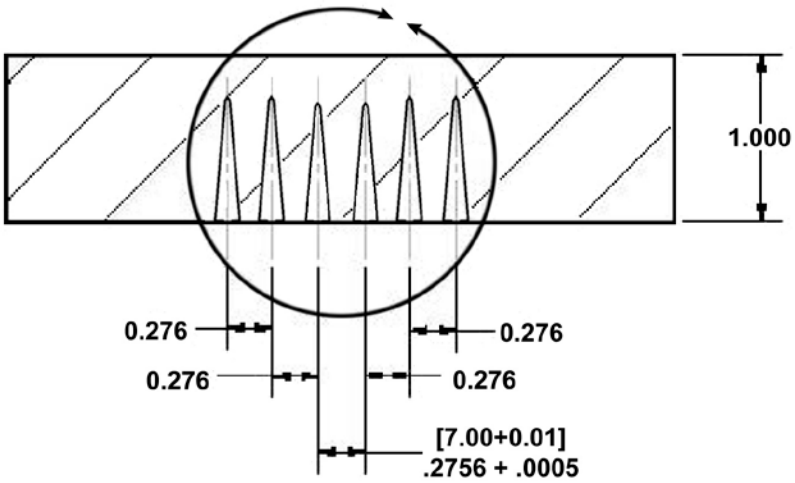

Figure 12. Cross section drawing of thermal calibration block machined from HDPE and Macor for TECP. The outer four holes are purposely oversized to accommodate the non-sensing needles while ensuring good thermal contact between the sensing needles and the block material.

again inserted until the needles were fully immersed, and the PEEK shoulders were not. The HDPE and Macor samples were machined to accommodate the four TECP needles.

A total of six needle holes were machined into the HDPE and Macor blocks, with the center two holes purposely cut slightly under-sized to ensure that the cones of needles 1 and 2 cone made solid thermal contact with the material (Figure 12). This resulted in a small gap between the PEEK shoulder and the calibration block. Before inserting the TECP into the Macor and HDPE blocks, all of the holes were completely filled with DI water to promote thermal contact between the needles and the material. The excess water that was forced from the holes during the insertion of the TECP was removed from the surface of the material block with a pipette. After insertion into each material, the TECP/material system was allowed to come into thermal equilibrium before data were collected. Additionally, between repeated measurements on the same sample, the TECP/material system was also allowed to come back to thermal equilibrium after introduction of the preceding heat pulse.

For each thermal properties measurement, the TECP control software was configured to record the output of the board temperature sensor, the three needle thermocouples, and the heater current sense resistor each second for 160 s. A 60 second heat pulse was applied to needle 1 after an initial 10 second buffer period with no heat. After cessation of the heat pulse, 90 s of cooling data were recorded. Each thermal property measurement was repeated at least twice in each material. For the glycerol, the needles were removed and re-inserted into the same sample between measurements. For the stabilized water, the needles were removed from the first sample and inserted into an identical, virgin sample between measurements. For the EPS, the needles were removed and inserted into a virgin section of the same block of the material. For the HDPE sample, the needles were removed from the sample, and the orientation of the sample was reversed so that needle 1 was in the hole formerly occupied by needle two. For the Macor sample, two measurements were made in the original orientation, and two in the reversed orientation for a total of four measurements.

Data analysis

Carslaw and Jaeger, (1959 p. 258-262) modeled the temperature surrounding an infinite line heat source with constant heat output and zero mass, in an infinite medium. When a

quantity of heat, Q (J m^{-1}) is instantaneously applied to the line heat source, the temperature rise at radial distance, r (m) from the source is

$$\Delta T = \frac{Q}{4\pi\,\kappa\,t}\exp\left(\frac{-r^2C}{4\kappa t}\right) \tag{2}$$

where κ is the thermal conductivity (W m^{-1} K^{-1}), C is the volumetric heat capacity (J m^{-3} K^{-1}), and t is time (s). If a constant amount of heat is applied to a zero mass heater over a period of time, rather than as an instantaneous pulse, the temperature response is

$$\Delta T = -\frac{q}{4\pi\,\kappa}Ei\left(\frac{-r^2C}{4\kappa t}\right) \qquad 0 < t \le t_1 \tag{3}$$

where q is the rate of heat dissipation (W/m), t_1 is the heating time, and Ei is the exponential integral. The temperature change after the heat is turned off is given by:

$$\Delta T = -\frac{q}{4\pi\,\kappa}\left[-Ei\left(\frac{-r^2C}{4\kappa t}\right) + Ei\left(\frac{-r^2C}{4\kappa(t-t_1)}\right)\right] \qquad t > t_1 \tag{4}$$

Material thermal properties are determined by fitting the time series temperature data during heating to Eq. (2), and during cooling to Eq. (3). Thermal conductivity and heat capacity can be obtained from the temperature of the heated needle (single needle), with r taken as the radius of the needle (1 mm). Heat capacity and thermal conductivity are also obtained by fitting equations 2 and 3 to the temperatures measured at the adjacent needle 7 mm from the heated needle.

A significant challenge in getting reliable results from the data was the fitting of equations (2) and (3) to the data. The non-linear Solver in Microsoft Excel was tried, as well as the method described by Marquardt (1963) and a multi-stage Monte Carlo (MSMCO) method described by Conley (1985). Both Solver and the Marquardt method gave results that depended on the starting values used to obtain the solutions. In other words, they located local minima, but had difficulty finding a global minimum. The MSMCO method was able to find the global minimum, but was fairly slow in converging to an accurate set of model values. In the end, the MSMCO method was used to obtain values close to the global minimum, and then the Marquardt method was used to find the final values. The exponential integral function was approximated using formulae from Abramowitz and Stegun (1972). The MSMCO-Marquardt algorithm was programmed into an MS Excel macro (*TECP thermal properties solver tool.xls*, Input tab). In this macro, the temperature of the fourth needle (farthest from the heated needle) is used as a temperature reference, as it is unaffected by the heat pulse from the heated needle during the duration of the measurement. This method also has the advantage of removing the effects of thermal drift of the bulk material during the measurement.

The outputs of the solver function in *TECP thermal properties solver tool.xls* are κ_1 and C_1, which are the thermal conductivity and volumetric heat capacity measured at the heated needle (needle 1), and κ_2 and C_2, which are thermal conductivity and volumetric heat capacity measured at the adjacent needle (needle 2). The measured values for κ and C are inherently inaccurate due to the departure of the TECP needles from the ideal case

of an infinite line heat source. However, the true thermal properties can be determined if calibration is performed in materials of known thermal properties as described here. The material thermal conductivity and heat capacity are determined by:

$$\kappa_{meas} = c1*\kappa_1 + c2*\kappa_2 + c3*C_1 + c4*C_2 + c5 \quad (5)$$

and

$$C_{meas} = c6*\kappa_1 + c7*\kappa_2 + c8*C_1 + c9*C_2 + c10 \quad (6)$$

The calibration coefficients [c1... c10] are determined by minimizing the error between known material κ and C values, and the values of κ_{meas} and C_{meas} determined from κ and C in eqs. (5 and 6), using the non-linear solver program in Excel (*TECP thermal properties solver tool.xls*, least squares solver tabs).

Results

Values for κ_1, κ_2, C_1 and C_2, generated from the MSMCO-Marquardt Excel macro for the 5 materials tested are shown in Table 6 and 7. Using these values to generate the calibration coefficients for eqs. (5 and 6) resulted in the calibration equations:

$$\kappa_{meas} = 0.617*\kappa_1 + 0.188*\kappa_2 + 0.039*C_1 - 0.015*C_2 - 0.118 \quad (7)$$

and

$$C_{meas} = 2.637*\kappa_1 - 0.747*\kappa_2 + 0.717*C_1 + 0.559*C_2 - 2.186 \quad (8)$$

for unit #004 and

$$\kappa_{meas} = 0.800*\kappa_1 + 0.105*\kappa_2 + 0.039*C_1 - 0.038*C_2 - 0.092 \quad (9)$$

and

$$C_{meas} = 2.411*\kappa_1 - 1.338*\kappa_2 - 0.014*C_1 + 0.713*C_2 - 0.883 \quad (10)$$

for unit #012.

Table 7. Thermal conductivity (κ, W m^{-1} K^{-1}) and heat capacity (C, MJ m^{-3} K^{-1}) values measured at needle 1 and 2 with TECP unit #012. The predicted values of κ and C are generated from equations 9 and 10, and the known values of κ and C are taken from literature or other sources.

Material	κ_1	κ_2	C_1	C_2	κ_{meas}	C_{meas}	κ_{known}	C_{known}
EPS	0.107	0.178	1.832	1.330	0.033	0.060	0.033	0.063
EPS 2	0.105	0.178	1.861	1.347	0.032	0.066		
Glycerol	0.508	0.503	2.457	4.605	0.289	2.920	0.285	2.960
Glycerol 2	0.480	0.436	2.767	4.133	0.289	2.600		
Water	0.889	0.910	2.485	6.131	0.580	4.382	0.606	4.170
Water 2	0.929	0.899	2.298	5.889	0.612	4.321		
Macor	1.630	2.395	1.188	3.238	1.387	2.136	1.401	2.020
Macor 2	1.648	2.561	1.182	3.368	1.413	2.050		
Macor 3	1.655	2.623	1.239	3.287	1.431	1.924		
Macor 4	1.639	2.506	1.243	3.168	1.411	1.958		
HDPE	0.667	0.891	2.246	3.104	0.506	1.718	0.513	1.691
HDPE2	0.669	0.885	2.166	3.062	0.505	1.701		

Tables 6 and 7 also show the known and predicted thermal properties values of the materials measured in the calibration routine.

B. January 2007 Calibration

Overview

During the January 2007 re-calibration of #012, a brief investigation was conducted to quantify any possible changes in the thermal properties function.

Experimental

TECP unit #012 originally underwent a full calibration of its thermal properties function in May 2006. During the January, 2007 re-calibration of the EC function, the thermal properties function of unit #012 was re-checked in the same thermal properties standard

Table 6. Thermal conductivity (κ, W m^{-1} K^{-1}) and heat capacity (C, MJ m^{-3} K^{-1}) values measured at needle 1 and 2 with TECP unit #004. The predicted values of κ and C are generated from equations 7 and 8, and the known values of κ and C are taken from literature or other sources.

Material	κ_1	κ_2	C_1	C_2	κ_{meas}	C_{meas}	κ_{known}	C_{known}
EPS	0.110	0.199	1.741	1.539	0.033	0.065	0.033	0.063
EPS 2	0.112	0.202	1.727	1.545	0.034	0.061		
Glycerol	0.498	0.526	1.815	5.149	0.283	2.913	0.285	2.96
Glycerol 2	0.517	0.534	1.669	5.097	0.291	2.823		
Water	0.936	1.071	1.077	7.232	0.595	4.296	0.606	4.17
Water 2	0.951	1.125	1.086	7.348	0.614	4.367		
Water 3	0.942	1.035	1.131	6.728	0.602	4.097		
Macor	1.629	2.846	0.409	3.095	1.391	2.008	1.401	2.02
Macor 2	1.636	2.832	0.401	3.149	1.392	2.059		
Macor 3	1.682	2.947	0.351	3.085	1.441	2.024		
Macor 4	1.634	2.904	0.377	3.151	1.404	1.986		
HDPE	0.683	1.062	1.268	3.484	0.501	1.679	0.513	1.691
HDPE2	0.694	1.122	1.199	3.627	0.514	1.693		

Table 8. Thermal conductivity (κ, W m^{-1} K^{-1}) and heat capacity (C, MJ m^{-3} K^{-1}) measured with TECP unit #012 during May 06 and Jan 07. The subscripts 06 and 07 indicate the calibration that was applied. In both cases, the calibration coefficients were applied to the raw data collected in May 2006. Significant changes are shaded.

Material	$\kappa_{meas\ 06}$	$\kappa_{meas\ 07}$	κ_{known}	$C_{meas\ 06}$	$C_{meas\ 07}$	C_{known}
EPS	0.033	0.034	0.033	0.060	0.003	0.063
EPS 2	0.032	0.033		0.066	0.022	
Glycerol	0.289	0.283	0.285	2.600	3.043	2.96
Glycerol 2	0.289	0.277		2.600	2.805	
Water	0.580	0.582	0.606	4.382	4.458	4.17
Water 2	0.612	0.604		4.321	4.286	
Macor	1.387	1.523	1.401	2.136	1.719	2.02
Macor 2	1.413	1.577		2.050	1.696	
Macor 3	1.431	1.605		1.924	1.610	
Macor 4	1.411	1.566		1.958	1.600	
HDPE	0.506	0.541	0.513	1.718	1.753	1.691
HDPE2	0.505	0.538		1.701	1.703	

materials as described in the previous document. In addition, a abbreviated calibration of unit #010 was conducted. The same apparatus and experimental protocols were used in the Jan 07 trial as were described for the May 06 trial.

Results

The data collected during the new thermal properties calibration check experiment were analyzed in the same manner as described for the May 06 trial, producing a new set of calibration coefficients [c1... c10]. To determine if change occurred in the thermal properties calibration resulting from the conformal coating, the Jan 07 calibration coefficients were applied to the raw data set collected in May 06. Table 8 shows the thermal properties calculated from the May 06 raw data (κ_1, κ_2, C_1, C_2) with the May 06 and Jan 07 calibration coefficients applied. It is apparent from the data shaded in Table 8 that the predicted values of volumetric heat capacity in the EPS and volumetric heat capacity and thermal conductivity in the Macor glass ceramic changed between trials. In the case of the EPS, this material has a volumetric heat capacity well outside the range that TECP is required to measure (0.4 to 4 MJ m^{-3} K^{-1}), and is outside the range which TECP can effectively resolve, so the deviation here is no surprise. In the case of the Macor, during the second calibration period, a possible mechanism for change in the measured thermal properties was observed.

During the first measurement period, water was used to thermally bridge any gaps that were present between the TECP needles and the walls in the conical holes in the Macor. After the May 06 calibrations, the water was not removed from the needle holes, and the Macor block was sealed in an airtight bag during the interim period. Water was still present in the holes when the sample was unpacked for the Jan 07 calibration. It is possible that the water infiltrated into the porous ceramic matrix over time and changed the thermal properties of the Macor in the vicinity of the measurement. Hence, it is recommended that the original calibration coefficients in equations 9 and 10 be applied to thermal properties data from unit #012.

Values for κ_1, κ_2, C_1 and C_2, generated from the MSMCO-Marquardt Excel macro for the 5 materials tested are shown in Table 9. Using these values to generate the calibration coefficients for eqs. (5 and 6) resulted in the calibration equations:

$$\kappa_{meas} = 0.622*\kappa_1 + 0.041*\kappa_2 - 0.201*C_1 - 0.011*C_2 + 0.324 \quad (11)$$

and

$$C_{meas} = 2.14*\kappa_1 - 0.956*\kappa_2 + 0.730*C_1 + 0.681*C_2 - 2.120 \quad (12)$$

for unit #010.

Table 9 also shows the known and predicted thermal properties values of the materials measured in the calibration routine.

Table 9. Thermal conductivity (κ, W m^{-1} K^{-1}) and heat capacity (C, MJ m^{-3} K^{-1}) values measured at needle 1 and 2 with TECP unit #010. The predicted values of κ and C are generated from equations 9 and 10, and the known values of κ and c are taken from literature or other sources.

Material	κ_1	κ_2	C_1	C_2	κ_{meas}	C_{meas}	κ_{known}	C_{known}
EPS	0.110	0.206	1.681	1.340	0.033	0.063	0.033	0.063
Glycerol	0.530	0.643	1.621	4.971	0.285	2.974	0.285	2.96
Water	0.912	0.951	1.211	6.376	0.606	4.158	0.606	4.17
Macor	1.755	2.597	0.381	3.780	1.401	2.018	1.401	2.02
HDPE	0.752	0.669	1.316	2.753	0.513	1.693	0.513	1.691

VI. Electrical Conductivity Function Calibration

A. May 2006 Calibration

Overview

The objectives of this procedure were two fold. First, the relationship between the TECP EC function output and the known resistance across the sensing needles was characterized for each unit. Second, aqueous EC standard solutions were used to find the probe constant vs. resistance function for each unit. By combining these two functions, the EC of the bulk medium surrounding the needles can be accurately determined.

Experimental

Part 1

Both TECP flight units (#004 and #012) were placed in the Delta Design controlled temperature chamber in the aluminum thermal buffer chamber. Copper blocks machined at the same cone angle as the TECP needles were used to make electrical contact between the TECP EC measurement needles and two clip-type leads that were routed through mouseholes to the exterior of the Delta Design chamber. The resistance of the leads was measured at 0.06 Ω, and has been neglected in the following analysis. The clip leads were use to sequentially connect the TECP EC needles across a series 24 of axial lead resistors ranging from 50 Ω to 250 MΩ. The resistance of each of the axial lead resistors was measured just prior to each TECP measurement with a calibrated Agilent multimeter (See AIDS for model number and calibration information). To allow EC circuit settling,

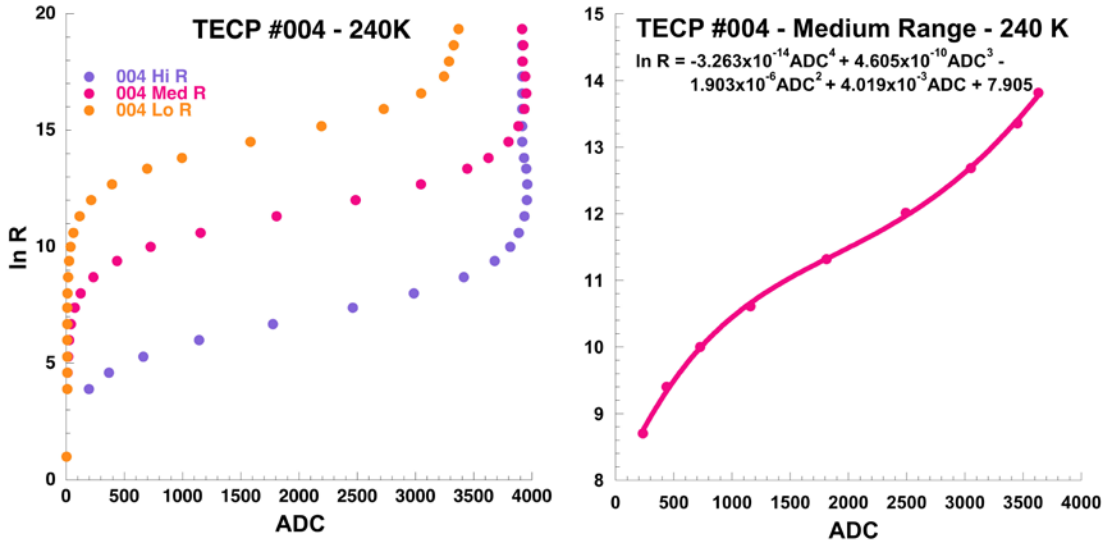

Figures 13 and 14. Example TECP output for all three measurement ranges over the full set of tested resistances (left). Example of relationship between TECP output and resistance (right). Note that the *y*-axis units are on a natural log scale.

data were collected across each resistor for 120 seconds per EC measurement range. The average of the last 10 seconds of TECP output for each measurement range has been used in all subsequent analyses. This process was repeated at five different TECP temperatures spanning temperature range of 160K to 323 K (-113°C to 50°C).

Part 2

Measurements were taken with each TECP unit in a series of six aqueous EC standard solutions ranging from 1 to 10,000 µS/cm. The EC solutions were poured to 500 ml in a 600 ml Pyrex beaker. All experiments were performed in the dry box with the TECP lowered into the solutions with the translation stage until the metal needles were fully submerged. The PEEK shoulders were not submerged in the solution. Measurements began with the 1 µS/cm sample (DDI water), and progressed to the highest salt concentration sample. The TECP needles were wiped dry and wiped with an isopropyl alcohol clean room wipe between samples. Before measuring with the TECP, the EC of each sample was measured with a calibrated Orion multi meter and EC cell (see AIDS for model numbers and calibration information). In the special case of the 1 µS/cm sample, where a very small amount of salt contamination would affect the EC of the sample significantly, the TECP was first dipped into the sample and removed, then the EC was measured with the Orion meter, and then the TECP was placed back into the sample and a measurement was taken. The TECP measurement again consisted of a 120 second measurement at each of the three EC measurement ranges. Again, the average of the last 10 seconds of TECP output for each measurement range has been used in all subsequent analyses.

Results

Part 1

The data collected across the 24 resistors were used to

Table 10. Ω limits for each TECP measurement range.

Range	Min Ω	Max Ω
Hi	--	6 kΩ
Med	6 kΩ	1MΩ
Low	156kΩ	--

construct a TECP output vs. resistance relationship for each EC measurement range (example data in Figure 13) at each temperature (data file: *TECP EC resistor data units 4 and 12.xls*). As is readily apparent from the example data in Figure 13, each measurement range has a finite useful range of resistances. These ranges are described in Table 10. After each data set was abbreviated to its useful range it was modeled as a 4th order polynomial function of TECP output vs. ln resistance (Figure 14, Table 11 and 12).

Some differences in the TECP output vs. R relationship were observed as the temperature of the TECP unit was changed in the Delta Design chamber. The differences were generally small (<10 ADC), but could be as large as 30 ADC at high resistance loads. Additionally, the response of the low EC range measurement became unpredictable at the very highest resistances during the 50°C measurements. For the following analyses, the data collected at 7°C have been used to predict the low EC resistance at all temperatures >7°C.

Part 2

Preliminary characterizations indicated that the TECP probe constant (geometric factor) varies as a function of the measured resistance. The known resistance vs. output functions determined in Part 1 were used in conjunction with the measurements in EC standard solutions in Part 2 to determine the probe constant vs. resistance relationship (data files: *TECP # 4 EC probe constant.xls* and *TECP # 12 EC probe constant.xls*). The probe constant is calculated by:

$$C_p = \frac{\left(\frac{1}{R}\right) * 1e^6}{EC} \tag{13}$$

Where C_p is the probe constant (cm), *R* is the measured resistance (Ω), and *EC* is the electrical conductivity of the sample (µS/cm). The probe constant vs. resistance functions are shown in Figures 15 and 16. Only the lowest EC solution (DDI water) fell within the useful resistance range of the low EC function, so a cell constant vs. measured resistance relationship could not be determined for the low EC function. The single point cell constant has been applied to all low EC function data described here ($C_{p,low}$ unit #004 = 3.79, $C_{p,low}$ unit #012 = 2.96).

Table 11. Polynomial fits for TECP #004, Ω vs. ADC for each EC range at the tested temperatures. The *y* variable is ln R, and *x* = TECP ADC output. **Note that the calibration functions in Figure 18 should be applied to the EC Low range output > 2750 ADC.**

T (K)	
	Hi range
160	$-8.341\text{x}10^{-14}x^4 + 8.237\text{x}10^{-10}x^3 - 2.751\text{x}10^{-6}x^2 + 4.743\text{x}10^{-3}x + 3.136$
200	$-7.892\text{x}10^{-14}x^4 + 7.927\text{x}10^{-10}x^3 - 2.691\text{x}10^{-6}x^2 + 4.718\text{x}10^{-3}x + 3.128$
240	$-7.809\text{x}10^{-14}x^4 + 7.858\text{x}10^{-10}x^3 - 2.673\text{x}10^{-6}x^2 + 4.699\text{x}10^{-3}x + 3.136$
280	$-7.742\text{x}10^{-14}x^4 + 7.807\text{x}10^{-10}x^3 - 2.661\text{x}10^{-6}x^2 + 4.690\text{x}10^{-3}x + 3.139$
323	$-7.769\text{x}10^{-14}x^4 + 7.820\text{x}10^{-10}x^3 - 2.662\text{x}10^{-6}x^2 + 4.689\text{x}10^{-3}x + 3.141$
	Mid range
160	$-3.248\text{x}10^{-14}x^4 + 4.654\text{x}10^{-10}x^3 - 1.922\text{x}10^{-6}x^2 + 4.037\text{x}10^{-3}x + 7.918$
200	$-3.171\text{x}10^{-14}x^4 + 4.536\text{x}10^{-10}x^3 - 1.885\text{x}10^{-6}x^2 + 4.004\text{x}10^{-3}x + 7.910$
240	$-3.263\text{x}10^{-14}x^4 + 4.605\text{x}10^{-10}x^3 - 1.903\text{x}10^{-6}x^2 + 4.019\text{x}10^{-3}x + 7.905$
280	$-3.128\text{x}10^{-14}x^4 + 4.498\text{x}10^{-10}x^3 - 1.877\text{x}10^{-6}x^2 + 4.000\text{x}10^{-3}x + 7.901$
323	$-3.100\text{x}10^{-14}x^4 + 4.478\text{x}10^{-10}x^3 - 1.873\text{x}10^{-6}x^2 + 3.998\text{x}10^{-3}x + 7.901$
	Low range
160	$3.433\text{x}10^{-13}x^4 - 1.813\text{x}10^{-9}x^3 + 2.535\text{x}10^{-6}x^2 + 9.912\text{x}10^{-4}x + 11.85$
200	$3.451\text{x}10^{-13}x^4 - 1.826\text{x}10^{-9}x^3 + 2.565\text{x}10^{-6}x^2 + 9.698\text{x}10^{-4}x + 11.85$
240	$2.342\text{x}10^{-13}x^4 - 1.116\text{x}10^{-9}x^3 + 1.133\text{x}10^{-6}x^2 + 1.971\text{x}10^{-3}x + 11.66$
280	$1.111\text{x}10^{-13}x^4 - 1.938\text{x}10^{-10}x^3 + 9.454\text{x}10^{-7}x^2 + 3.561\text{x}10^{-3}x + 11.35$
323	$2.909\text{x}10^{-13}x^4 - 1.240\text{x}10^{-9}x^3 + 9.917\text{x}10^{-7}x^2 + 2.302\text{x}10^{-3}x + 11.57$

Table 12. Polynomial fits for TECP #004, ∧ vs. ADC for each EC range at the tested temperatures. The *y* variable is ln R, and *x* = TECP ADC output.

T (K)	
	Hi range
160	$-7.301\text{X}10^{-14}x^4 + 7.481\text{X}10^{-10}x^3 - 2.578\text{X}10^{-6}x^2 + 4.610\text{X}10^{-3}x + 3.153$
200	$-7.445\text{X}10^{-14}x^4 + 7.584\text{X}10^{-10}x^3 - 2.609\text{X}10^{-6}x^2 + 4.648\text{X}10^{-3}x + 3.133$
240	$-7.655\text{X}10^{-14}x^4 + 7.765\text{X}10^{-10}x^3 - 2.662\text{X}10^{-6}x^2 + 4.706\text{X}10^{-3}x + 3.116$
280	$-7.488\text{X}10^{-14}x^4 + 7.622\text{X}10^{-10}x^3 - 2.619\text{X}10^{-6}x^2 + 4.657\text{X}10^{-3}x + 3.136$
323	$-7.562\text{X}10^{-14}x^4 + 7.683\text{X}10^{-10}x^3 - 2.637\text{X}10^{-6}x^2 + 4.677\text{X}10^{-3}x + 3.132$
	Mid range
160	$-3.378\text{X}10^{-14}x^4 + 4.707\text{X}10^{-10}x^3 - 1.930\text{X}10^{-6}x^2 + 4.042\text{X}10^{-3}x + 7.915$
200	$-3.039\text{X}10^{-14}x^4 + 4.420\text{X}10^{-10}x^3 - 1.857\text{X}10^{-6}x^2 + 3.980\text{X}10^{-3}x + 7.905$
240	$-2.987\text{X}10^{-14}x^4 + 4.372\text{X}10^{-10}x^3 - 1.843\text{X}10^{-6}x^2 + 3.967\text{X}10^{-3}x + 7.900$
280	$-2.987\text{X}10^{-14}x^4 + 4.377\text{X}10^{-10}x^3 - 1.847\text{X}10^{-6}x^2 + 3.973\text{X}10^{-3}x + 7.896$
323	$-3.036\text{X}10^{-14}x^4 + 4.423\text{X}10^{-10}x^3 - 1.861\text{X}10^{-6}x^2 + 3.993\text{X}10^{-3}x + 7.888$
	Low range
160	$2.481\text{X}10^{-13}x^4 - 1.188\text{X}10^{-9}x^3 + 1.252\text{X}10^{-6}x^2 + 1.901\text{X}10^{-3}x + 11.68$
200	$9.238\text{X}10^{-14}x^4 - 1.176\text{X}10^{-10}x^3 - 1.089\text{X}10^{-6}x^2 + 3.672\text{X}10^{-3}x + 11.32$
240	$2.362\text{X}10^{-13}x^4 - 1.171\text{X}10^{-9}x^3 + 1.328\text{X}10^{-6}x^2 + 1.776\text{X}10^{-3}x + 11.69$
280	$3.370\text{X}10^{-13}x^4 - 1.725\text{X}10^{-9}x^3 + 2.298\text{X}10^{-6}x^2 + 1.173\text{X}10^{-3}x + 11.79$
323	$3.496\text{X}10^{-13}x^4 - 1.706\text{X}10^{-9}x^3 + 2.082\text{X}10^{-6}x^2 + 1.446\text{X}10^{-3}x + 11.73$

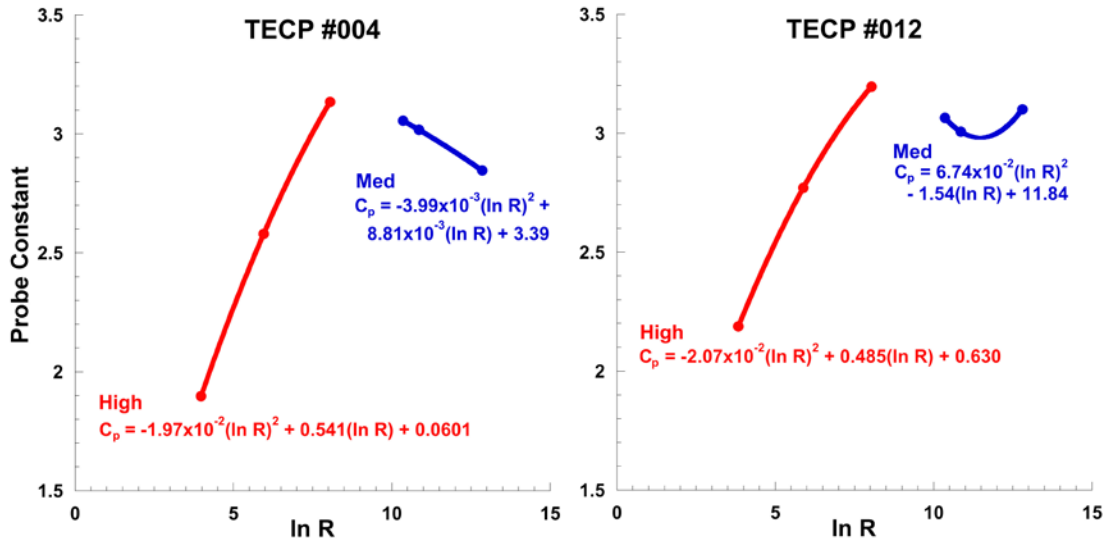

Figures 15 and 16. The Probe Constants for units #004 (Figure 15, left), and #012 (Figure 16, right).

B. EC Calibration Shift Analysis

Overview

During post conformal coat testing, it was noticed that the TECP flight unit (#004) had experienced a calibration shift in the electrical conductivity (EC) function. This calibration shift was presumably a result of the application of the conformal coating. However, since unit #004 was attached to the robot arm, it was unavailable for re-calibration. So, the unit which was the flight spare at that time (unit #012) was re-calibrated with two possible goals in mind. First, if unit #012 changed in a similar manner to #004, then a mechanism for the change can possibly be deduced, and a correction can be applied #004. In the event that the changes in the units were not identical, then #012 is to be re-calibrated, and substituted for #004 when the TECP is removed from the RA to allow installation of the ISAD.

Experimental

Full calibrations of the EC function of both units were conducted in May, 2006. The results of the calibrations were documented in *Flight EC calibration.doc*, submitted to JPL by Decagon Devices. After conformal coating, the flight unit (#004) was functionally tested by JPL personnel. The functional test was comprised of measurements in all three EC ranges while the sensing needles were open circuited, and additional individual tests of the three EC ranges over precision resistors picked to fall within each EC functional range. The results of these tests were compared to results collected during functional testing before conformal coating over the same resistors/open circuit conditions. The apparent change in the TECP reading over the functional testing conditions prompted an analysis of the change in the flight spare, consisting of functional testing over the same resistors/open circuit conditions and comparing to data collected during functional testing before conformal coating on that unit.

Table 13. Pre-coating and post coating ADC test data from TECP units #004 and #012 EC function, and the absolute difference (Δ)

Condition	#004 Pre-	#004 Post-	#004 Δ	#012 Pre-	#012 Post-	#012 Δ
Low EC open	3273	3831	558	3396.5	3429	32.5
Mid EC open	3928	3930	2	3946.9	3949	2.1
Hi EC open	3931	3935	4	3949.8	3947.2	-2.6
Low EC 3.91MΩ	2144	2161	17	2200	2210	10
Mid EC 165.2kΩ	2493	2492	-1	2506.3	2506.1	-0.2
Hi EC 1.624kΩ	2461	2461	0	2474	2475.4	1.4

Results

It is apparent from the results in Table 13 that the change in TECP output was not the same between units. The change is small, and similar in the medium and high EC ranges, but the change becomes significant and dissimilar between units in the Low EC range, especially as the resistance becomes very high (open circuit).

Since the majority of the TECP measurements will likely be in the low EC range, it was decided that unit #012 should be re-calibrated, and substituted for #004. However, after this was accomplished, unit #012 was subsequently mis-mated and powered up during ATLO, thus requiring unit #004 to be returned to flight service.

C. January 2007 Calibration

Overview

As outlined in the section B. above, a full EC re-calibration was performed on unit #012 in preparation for its replacement of #004 as the flight unit. Additionally, unit #010 was

Table 14. Polynomial fits for unit #010 resistance vs. output for the three EC measurement ranges at the tested temperatures. The *y* variable is ln R, and the *x* variable is TECP output.

T (K)	

Table 15. January 2007 polynomial fits for unit #012 resistance vs. output for the three EC measurement ranges at the tested temperatures. Note that the *y* variable is ln R, and the *x* variable is TECP output.

T (K)	Hi range
160	$-7.642\times10^{-14}x^4 + 7.733\times10^{-10}x3 - 2.640\times10^{-6}x^2 + 4.662\times10^{-3}x + 3.145$
200	$-7.513\times10^{-14}x^4 + 7.641\times10^{-10}x3 - 2.624\times10^{-6}x^2 + 4.659\times10^{-3}x + 3.133$
240	$-7.538\times10^{-14}x^4 + 7.668\times10^{-10}x^3 - 2.633\times10^{-6}x^2 + 4.671\times10^{-3}x + 3.132$
280	$-7.559\times10^{-14}x^4 + 7.690\times10^{-10}x^3 - 2.641\times10^{-6}x^2 + 4.684\times10^{-3}x + 3.125$
323	$-7.567\times10^{-14}x^4 + 7.684\times10^{-10}x^3 - 2.636\times10^{-6}x^2 + 4.675\times10^{-3}x + 3.134$
	Mid range
160	$-3.179\times10^{-14}x^4 + 4.540\times10^{-10}x^3 - 1.884\times10^{-6}x^2 + 3.997\times10^{-3}x + 7.921$
200	$-2.986\times10^{-14}x^4 + 4.387\times10^{-10}x^3 - 1.851\times10^{-6}x^2 + 3.976\times10^{-3}x + 7.905$
240	$-2.973\times10^{-14}x^4 + 4.374\times10^{-10}x^3 - 1.847\times10^{-6}x^2 + 3.973\times10^{-3}x + 7.901$
280	$-3.019\times10^{-14}x^4 + 4.412\times10^{-10}x^3 - 1.860\times10^{-6}x^2 + 3.993\times10^{-3}x + 7.887$
323	$-2.970\times10^{-14}x^4 + 4.380\times10^{-10}x^3 - 1.853\times10^{-6}x^2 + 3.990\times10^{-3}x + 7.888$
	Low range
160	$2.347\times10^{-13}x^4 - 1.194\times10^{-9}x^3 + 1.398\times10^{-6}x^2 + 1.725\times10^{-3}x + 11.73$
200	$2.998\times10^{-13}x^4 - 1.467\times10^{-9}x^3 + 1.734\times10^{-6}x^2 + 1.618\times10^{-3}x + 11.73$
240	$2.657\times10^{-13}x^4 - 1.267\times10^{-9}x^3 + 1.351\times10^{-6}x^2 + 1.866\times10^{-3}x + 11.68$
280	$2.625\times10^{-13}x^4 - 1.331\times10^{-9}x^3 + 1.619\times10^{-6}x^2 + 1.597\times10^{-3}x + 11.73$
323	$3.285\times10^{-13}x^4 - 1.653\times10^{-9}x^3 + 2.107\times10^{-6}x^2 + 1.361\times10^{-3}x + 11.76$

calibrated concurrently.

Experimental

The experimental equipment and methods used during the January 2007 calibration were identical to those described in section A. above.

Results

Tables 14 and 15 show the polynomial fits obtained for units #010 and #012 during the January 2007 calibration campaign. Figures 17 and 18 show the probe constant functions generated for units #010 and #012 during the January 2007 calibration campaign.

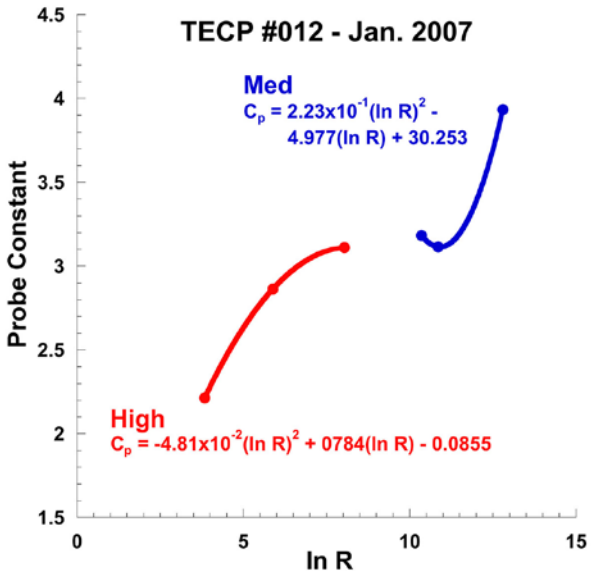

Figure 18 High and Medium range TECP EC probe constant functions for #012 derived during the January 2007 calibration campaign.

D. March 2007 calibration of unit #004

Overview

Due to the mis-mate and power up of unit #012, unit #004 was returned to flight duty in March of 2007. However, this unit was not included in the January 2007 calibration campaign and had not been re-calibrated after conformal coating tests indicated that there had been some change in the EC function response in the very high impedance range (see Table 13 above), so a quick calibration in the high impedance range was conducted.

Experimental

The March 2007 calibration was conducted at the Lockheed Martin facility in Denver, CO. A similar protocol to that outlined in part A. above was used. However, the set of resistors used was limited to just the high impedance (low EC) range. This was justified by the lack of change that was apparent in the Hi and Mid EC ranges (see Table 13 above). Additionally, due to time constraints, only three temperatures were included in the data gathering activities (200 K, 240 K, and 280 K).

Results

Figure 18 and Table 16 show the polynomial curve fits to the newly acquired high impedance test data. These curve fits supersede those presented in Table 11, and should be applied to any measurement resulting in a TECP Low range EC output >2750 ADC. In the lower impedance range, the default curve fits derived from the May 2006 calibration data and presented in Table 11 should be applied. It should also be noted that at impedances higher than the range presented in Figure 19, the TECP low range EC measurement becomes unstable, and should not be used. The upper end of the usable range for unit #004 is 3400 ADC, which represents an impedance of approximately 126 MΩ, or an EC of 2.1 nS/cm.

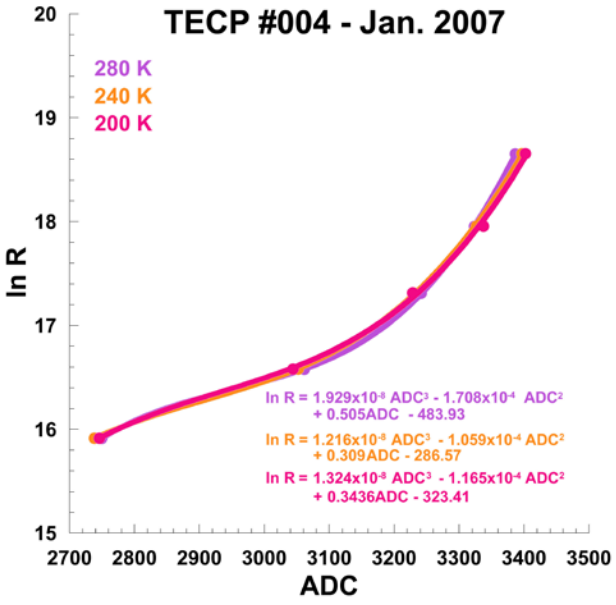

Figure 19. High impedance calibration data and curve fits for TECP #004 low range EC function at three temperatures. Data were collected during the March 2007 calibration campaign, and should be applied to any unit #004 low EC range output >2750 ADC.

Table 16. January 2007 polynomial fits for unit #004 resistance vs. output for the low EC measurement range at the tested temperatures.

T (K)	Low range
200	$1.324\text{x}10^{-8}x^3 - 1.165\text{x}10^{-4}x^2 + 0.345x - 323.41$
240	$1.216\text{x}10^{-8}x^3 - 1.059\text{x}10^{-4}x^2 + 0.309x - 286.57$
280	$1.929\text{x}10^{-8}x^3 - 1.708\text{x}10^{-4}x^2 + 0.505x - 483.93$

VII. Relative Humidity Function Calibration

Overview

Calibration of the TECP humidity function was carried out at the University of Washington Mars Atmospheric Simulation Facility (MASF) .

The humidity-sensing element of the TECP is a Panametrics MiniCap-2, a commercial capacitive polymer-based sensor whose performance at temperatures and frost-points below ~ 230 K was not well known. It is mounted on the TECP electronics board, directly beneath a hole in the TECP housing which is covered by a permeable Teflon membrane to allow air in while keeping dust out. The capacitance is proportional to the relative humidity of the air in contact with the sensor. By assuming that the temperature of the air is equal to the temperature of the electronics board (T_b), which is monitored with a calibrated thermistor, the absolute humidity (or water vapor concentration) can be determined.

The humidity calibration took place from March 25 to March 30, 2006. During this period, more than 50,000 measurements, at 5 to 30 second intervals, covering a wide range of T_f (-80°C to -10°C) and T_b (-65°C to +30°C) were collected. Most of the data were collected with the chamber containing CO_2 gas at a pressure of ~5 Torr (7mb), flowing through at ~200 sccm. A calibration curve for 3 of the 4 TECP-HS FM's was calculated as a six-parameter quadratic function of relative humidity and temperature. TECP FM #010 stopped functioning on March 28 and therefore was not calibrated.

Experimental

MASF Design & Operation

A custom test chamber - the TECP Calibration Chamber (TCC) – was designed and constructed to permit simultaneous calibration of the four Flight Models (FMs). The TCC was constructed using stainless steel and ceramic high-vacuum fittings to minimize adsorption and outgassing of water vapor.

TCC provides independent control of humidity, temperature, and pressure, and also simulates low wind speeds (Schneider 2001). The facility is an open, continuous flow system, which uses CO_2 from a standard high pressure bottle as the atmospheric simulant. The CO_2 first passes through a pressure regulator to reduce its pressure to about 0.1 MPa, and is then directed to the humidity generator, which contains a saturator, a dryer, and two MKS Instruments mass flow controllers which regulate the relative mass flows of the dry and wet gas streams, and further reduce the flow pressure to ~20 kPa.

The desired humidity is set by mixing the wet and dry CO_2 flows in the appropriate ratio. The frost/dew points of the saturated and dry flows are controlled by their temperature. In the saturator, the CO_2 flow passes over liquid water or ice, whose temperature is maintained within ±0.1 K by a Neslab RTE-4 circulating cooler. The dry flow is generated by passing CO_2 through a heat exchanger held at 195 K by immersion in a slurry of dry ice and ethanol. Since the atmospheric pressure on Mars is only ~600-1000 Pa, the flow is expanded to this pressure range by means of a sonic orifice. This expansion also decreases the concentration of water vapor to its final desired value.

The conditioned flow enters the test chamber located inside a low-temperature freezer (Environ-mental Equipment So-Low C-85-5) that maintains the desired Mars ambient temperature, controlled via LabVIEW software. After exiting the test chamber the gas passes through a Buck Research CR-1 chilled mirror hygrometer (B), which measures the frost point of the flow (Busen and Buck, 1995). Finally, the flow passes through a 195 K cold trap and into the vacuum pump. All interconnecting tubing (12.7 mm OD) and fittings are made of electro-polished stainless steel to minimize uncontrolled adsorption or desorption of water from internal surfaces.

The frost-point temperature (T_f), or absolute humidity, of the air flowing through the TCC was measured using a Buck CR-1 chilled-mirror hygrometer, which uses liquid nitrogen for mirror cooling and can measure T_f over the range 183 K to 303 K with an accuracy of ±0.3 K. Additionally, an EdgeTech DewPrime I chilled-mirror hygrometer was used. Both hygrometers have a NIST-traceable calibration for $T_f \geq 198$ K.

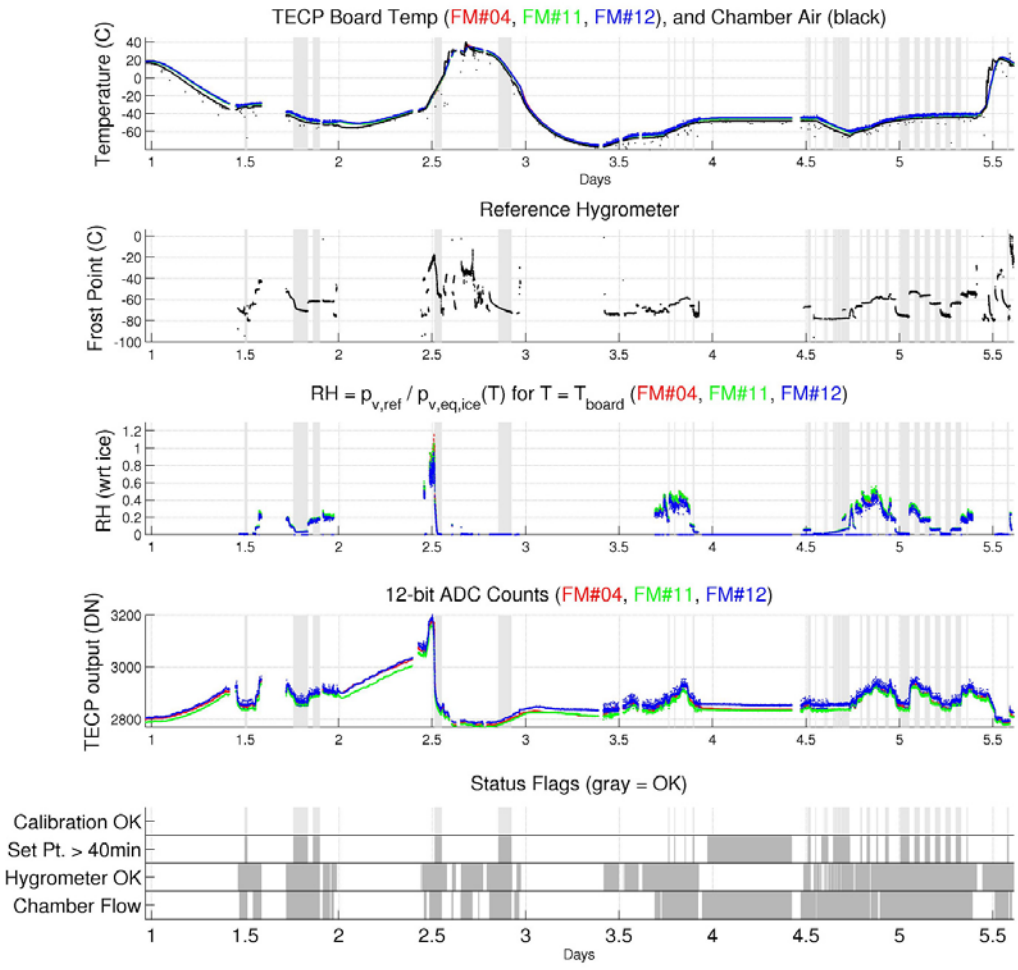

Figure 20 (A). Plots of the primary measured variables for the entire calibration run. The color code for each subplot is given in the title, and the light-gray shading indicates which data points were used for calibration. The dark-gray "bar-code" at the bottom of each plot indicates the status of several data quality flags used to select the final calibration dataset.

The MASF is a flow-through system, so the unavoidable hygroscopic materials such as the insulated lead wires were placed upstream of the TECP's to minimize any humidity changes between the TECP's and the reference hygrometer. The MASF also has a bypass line to monitor the humidity of the air before it enters the test chamber.

In-Flight Data

Because of the extreme difficulty of maintaining high relative humidity at the lowest calibration temperatures, the calibration data set was undesirably sparse for precisely the conditions that obtain during the overnight hours. In order to augment the calibration data set, flight data from sols 86, 91,103-104, and 122 were also included. Based upon observations from the Met Package Lidar, it is independently known that the Martian atmosphere was saturated throughout the lowest ~ 1 km after 2300h on each of these sols. Only data acquired simultaneously with lidar confirmation of ground fogs were used to augment the calibration data set.

In addition, the TECP R_H function was exercised during cruise to Mars, as part of the MECA functional checkout. The in-flight checkout was conducted on November 13, 2007, by which time the TECP had been exposed to vacuum for 94 days. Therefore, data from the in-flight checkout was included as a $R_H = 0$ data point.

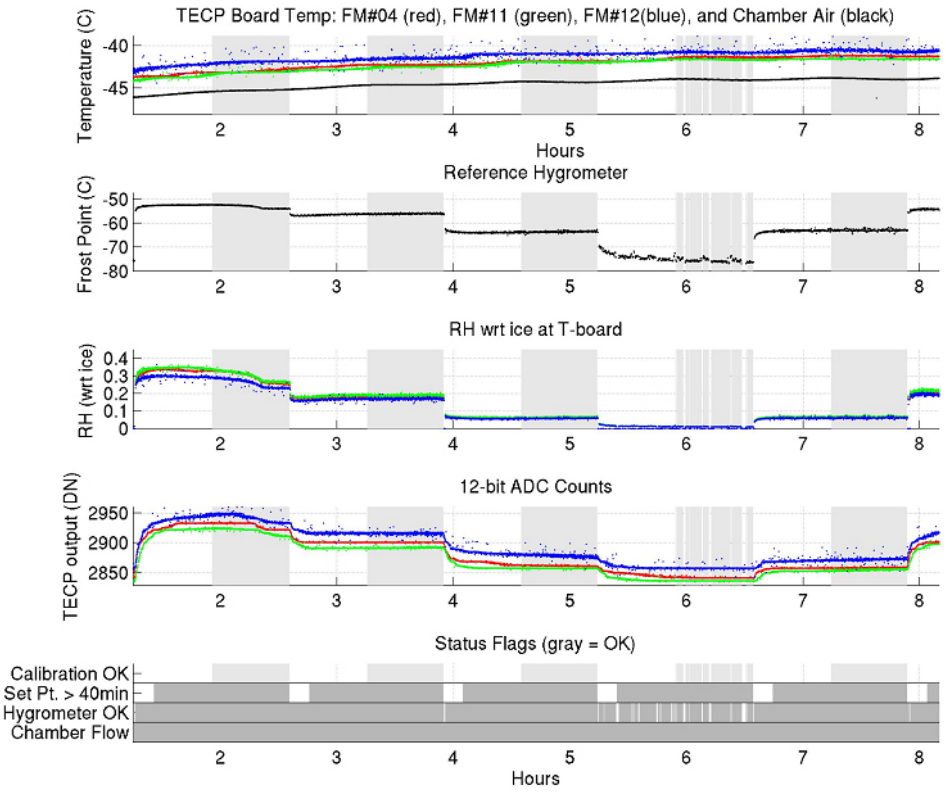

Figure 20 (B). Plots of the primary measured variables for a "zoomed-in" section of day 5. The color code for each subplot is given in the title, and the light-gray shading indicates which data points were used for calibration. The dark-gray "bar-code" at the bottom of each plot indicates the status of several data quality flags used to select the final calibration dataset.

Results

During calibration of the four TECP Flight Units, we collected more than 50,000 measurements, at 5 to 30 second intervals, covering a wide range of T_f (193 K to 263 K) and T_b (208 K to 303 K) (Figure 20 A). Most of the data were collected with the chamber containing CO_2 gas at a pressure of 650 Pa, flowing through at ~200 sccm. An example of the raw data from one set of measurements is shown in Figure 20B, which also illustrates the unexpectedly fast response time of the sensor to humidity changes (< 10 min).

Revised calibration function

A revised calibration function was generated in 2011 in order to correct for inaccuracies in the previous function at the lowest temperatures encountered during flight.
Because the original flight instrument calibration was performed against a pair of hygrometers that measured frost point (T_f), the revised calibration equation is also cast in terms of frost point.

Use of Flight Data

Due to resource limitations, it was not possible to calibrate the TECP R_H sensor in the laboratory at air temperatures < 208 K. The sensor response during flight was a smoothly continuous function down to the lowest temperatures detected, ~ 181 K. To improve the reliability and range of the calibration, the decision was made to use flight data, acquired during periods when the atmosphere is known to have been saturated. The following criteria were used to select the flight data for inclusion in the calibration:

1. The data were acquired after sol 70, (L_s = 108º) and between the hours of 0000h and 0400h LMST. During these periods, the LIDAR detected a regular pattern of cloud formation each night within the PBL. A shallow surface-based cloud formed near midnight (Mars local solar time), and a second cloud layer formed after 1 a.m. at heights around 4 km, because these were the coldest parts of the atmosphere (Whiteway *et al.,* 2009).
2. The TECP board temperature (T_b) varied by no more than 1K, and was within ± 1.5 K of the MET mast 1m temperature. This criterion assured that the humidity measurement, which is made at T_b, was acquired at the same temperature as the ambient air. The standard deviation assigned to the R_H = 1 flight data was $10^{-4}T_f$, which is not unreasonable compared to the laboratory calibration data.

	Pt 1	*Pt. 2*
L_s	115.9	133.4
Sol	86	122
S/C Clock Start	903802401.2873691	906999999.0888211
S/C Clock Stop	903804626.4754640	907002546.3552399
LMST Start	0.59519 h	1.0518 h
LMST Stop	1.19677 h	1.7405 h
n, Measurements	95	55
$\bar{x}$, ADC	2878.8	2856.1
σ, ADC	0.637	0.348
$\bar{x}$, T_b	192.98	181.64
σ, T_b	0.1488	0.1138

These criteria led to the inclusion of two sets of data in the calibration, as detailed in the table.

Although data were acquired during cruise (P_{H2O} = 0), that data could not be used in this calibration, since we are calibrating to T_f.

During flight, no data was

acquired at $T_b > 260$K. The original laboratory calibration however incorporated data acquired up to ~300 K. It was found that inclusion of this high-temperature calibration data adversely affected the goodness-of-fit metric (χ^2) in the T_b domain relevant to the mission data ($T_b \leq 260$ K). Therefore, laboratory calibration data acquired at $T_b > 280$ K were omitted from the data for fitting.

The final calibration equation for conversion of TECP R_H ADC and T_b to atmospheric frost point is

term1 = X_1*ADC^2;
term2 = X_2*ADC;
term3 = X_3*(ADC/T_b);
term4 = X_4* T_b^2;
term5 = X_5*T_b;
term6 = X_6;

T_f = term1+term2+term3+term4+term5+term6;

X_i = -0.00023947; 2.04253; -100.587; 0.0229374; -15.8257; -0.26369
χ^2 = 451946; σ = 2.64226

Revised Reduced Data Records (RDRs) released in July, 2011 utilize this new function. The data are expressed both in frostpoint and vapor pressure, utilizing the Goff-Gratch formalism for interconversion (Goff and Gratch 1946)

References

Abramowitz, M. and I. A. Stegun. 1972. *Handbook of mathematical functions.* Dover Publications, Inc., New York

Boynton, W. V., W. C. Feldman, S. W. Squyres T. H. Prettyman, J. Brückner, L. G.Evans, R. C.Reedy, R. Starr, J. R. Arnold, D. M. Drake, P. A. J. Englert, A. E. Metzger, I. Mitrofanov, J. I. Trombka, C.D 'Uston, H. Wänke, O. Gasnault, D. K. Hamara, D. M .Janes, R. L .Marcialis, S. Maurice, I. Mikheeva, G. J. Taylor, R.Tokar, C.Shinohara, Distribution of hydrogen in the near surface of Mars: Evidence for subsurface ice deposits, *Science,* **297,** 81-85, 2002

Busen, R., and Buck, A.L., "A High-Performance Hygrometer for Aircraft Use: Description, Installation, and Flight Data," J. Atmos .& Oceanic. Tech. 12, 73-84 (1995).

Carslaw, H.S. and J.C. Jaeger. *Conduction of Heat in Solids*. 2nd Edition. Oxford, London, 1959

Cobos, D.R., G.S. Campbell, and C.S. Campbell. 2006. Modified Line Heat Source for Measurement of Thermal Properties on Mars. *Thermal Conductivity 28/Thermal Expansion 16.*

Conley, W. 1985. Solving systems of equations with multi-stage Monte Carlo optimization. *Int. J. Systems Sci.* 16:1239-1248.

Ganic, E.N. and T. G. Hicks (eds.). 1991. *Essential Engineering Information and Data*. McGraw-Hill, New York.

Goff, J. A., and S. Gratch, Low-pressure properties of water from −160 to 212 °F, *Transactions of the American Society of Heating and Ventilating Engineers*, pp 95–122, presented at the 52nd annual meeting of the American Society of Heating and Ventilating Engineers, New York, 1946. Also see Smithsonian Meteorological Tables, 5th ed., pp. 350, 1984.

Hecht M. H. et al. (2003) AGU Fall 2003, Abstract #P41B-0404.

Jakosky, B. M., C. B. Farmer, The seasonal and global behavior of water in the Mars atmosphere: Complete global results of the Viking atmospheric water detector, *J. Geophys. Res.,* **87,** 2999-3019, 1982

Marquardt, D. W. An algorithm for least-squares estimation of nonlinear parameters. *J. Soc. Indust. Appl. Math.* 11:431-441, 1963

Mellon, M.T., W.C. Feldman & T.H. Prettyman. The presence and stability of ground-ice in the southern hemisphere of Mars. *Icarus* **169**, 324-340, 2004

MEPAG (2006) http://mepag.jpl.nasa.gov/reports/

Mitrofanov, I., D. Anfimov, A. Kozyrev, M. Litvak, A. Sanin, V. Tret'yakov, A. Krylov, V. Shvetsov, W. Boynton, C. Shinohara, D. Hamara, R. S. Saunders, Maps of subsurface hydrogen from the High Energy Neutron Detector, Mars Odyssey, *Science* **297**, 78-81, 2002

Paige D. A. The thermal stability of near-surface ground ice on Mars, *Nature,* **356**, 43-45, 1992

Schneider M. A. and Bruckner A. P. () Space Tech. and App. Int. Forum – STAIF 2003, ed. M.S. El-Genk, 1124-1132, 2003

Schorghofer N., O. Aharonson, Stability and exchange of subsurface ice on Mars, *J. Geophys. Res.,* **110**, E05003, 2005

Smith, M. D., The annual cycle of water vapor on Mars as observed by the Thermal Emission Spectrometer,*J. Geophys. Res.,***107**, doi:10.1029/2001JE001522, 2002

Tamppari L. K. et al. (2006) 2nd Wrkshp Mars Atm. Model. & Obs., Granada, Spain, 212. [**7**] Feldman W. C. et al. (2004) *JGR 109*, E09006.

Whiteway, J.A. et al, Mars Water-Ice Clouds and Precipitation, *Science* **325**, 68-70, 2009.